1. Reply to the reviewer 1#

We are very grateful to this referee comments, and we have carefully read and considered the referee's comments, and these comments are important for improving the quality of this manuscript. Based on these comments, we have made carefully modification and proofreading on the original manuscript, the detail modifications are mainly for the chapter - Abstract and Introduction, which have been reconstructed and rewrote, and description of the Wobaoshi Landslide's geological structure and characteristics have been modified and reconstructed, and language, grammar and professional terms in English also have been improved.

Please see the detailed revision, and we carefully proof-read the manuscript to minimize typographical, grammatical, and bibliographical errors, and the modified parts are marked in red in the revised manuscript.

Thank you very much for your suggestion and consideration, and we look forward to hearing from you.

Best regards,

Yimin Liu, Chenghu Wang and Pu wang.

Detailed revision for comments of reviewer 1#

1. *Language, in general is not good and some sentences are unclear. Some professional terms are incorrect. (comment 1)*

Modification:

For the unclear parts and unprofessional terms in the manuscript, we have made serious changes in English expression to ensure clearly presented, and proofreading also has been done, and the revised changes are in red in the manuscript.

For instance, "overall occurrence of the rock formation" has changed to "overall attitude of rockbed" in line 131, "planar graph" has changed to "topographic map" in Fig. 3 in line 136, "gage" has changed to "gauge" in line 200, 202, 204 and 205, "long-period" has changed to "long-term", "heavy rain" has changed to "periodic rain", "rainy season" has changed to "monsoon", "mechanical" has changed to "geomechanical", "field exploration" has changed to "field investigation", "starting" has changed to "initiation", "theorical" has changed to "theoretical" in the manuscript, and we have spelled all abbreviations and acronyms at their first mention in the main text, such as enhanced thematic mapper called ETM+, and digital elevation model called DEM in line 67 and 68. Thus, these descriptions will be more accurate and professional than before.

2. *Introduction, there is a little more information (what, where, why) and presentation of the main aim of the paper. Does the landslide threaten something? Why it is important to be studied? (comment 2)*

Modification:

This comment is very important for the paper, and the presentation of the main aim in original manuscript is lack of refinement and detailed narrative. Therefore, we modify and supplement the purpose and importance of this manuscript, firstly, the occurrence of plate-shaped translational landslides is often unexpected and covert; secondly, the field investigation and monitoring data for this kind of landslide is often absent, and the research on translational landslide lacks monitoring engineering and measured data on landslide physical parameters. Thus, demonstrating and validating the deformation and failure mode of the translational landslide in the theoretical analysis is difficult.

As shown observation point b and c in Fig. 2, the Wobaoshi landslide seriously threaten residential houses and highways, the houses had cracked and highways had uplifted, so this landslides seriously threatens the safety of people's property and transportation, thus it is necessary to research on it. This supplementary part is from line 181 to line 183. We added a photo of the house cracking in observation point b of Figure 2, and this photo was taken in a field investigation in the Wobaoshi landslide.

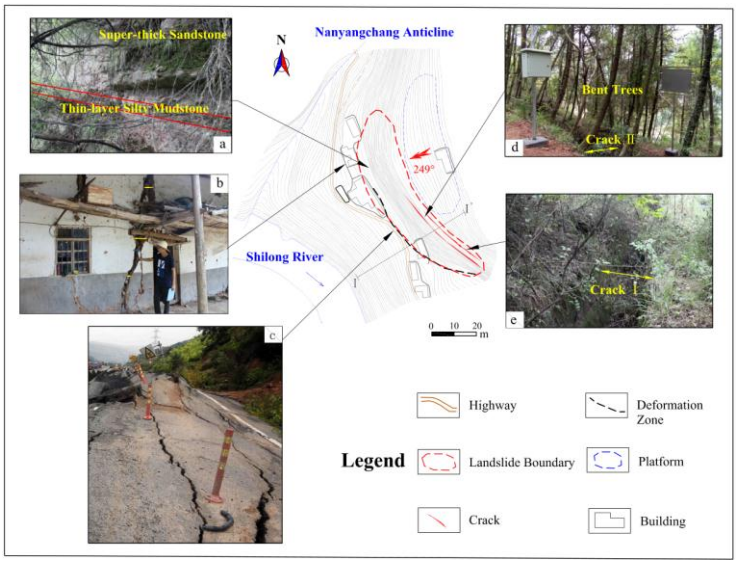

Fig. 2 Topographic map of the Wobaoshi landslide and photographs of observation points: (a) exposed bedrock at the front edge; (b) the houses had cracked at the front edge (c) the roadbed is pushed uplifted at the front edge; (d) crack II and bent trees; and (e) crack I.

Additionally, detail description and conclusion of characteristics and failure mode of the landslide in chapter – Introduction, have been transferred to the chapter – Results.

3. *In the Landslide characteristics the geological structure is not clearly presented. Monitoring results and numerical modeling results are clearly presented (graphs, models). (comment 3)*

Modification:

In origin manuscript, the Section 1 "Landslide characteristics" is not clearly presented like the comment said. Thus we reconstruct the Section 1 and especially make change on the forming conditions, especially the engineering geological conditions of this landslide. At the same time, some geological terms have been

corrected. Through the modification, we feel that geological structure and characteristics of the Wobaoshi landslide will be more clearly and accurate than the origin vision.

4. *Discussion is clearly written. The system of long-term gradual opening of the cracks and short-term opening and closing of cracks (blocks tilting) (very characteristic on the graphs) could be described more in detail. (comment 4)*

Modification:

The system of long-term cracks opening and short-term cracks closing is described in detail in Section 2.2 “Monitoring Data Analysis”, and the Section 4.1 “Deformation and Failure Mode Exploration” in discussion, is refined by the landslide monitoring data analysis in Section 2.2. And we have increased the relationship between the “Monitoring Data Analysis” and “Deformation and Failure Mode Exploration” in Section 4.1.

5. *Any possible mitigation measures or additional monitoring suggested? (comment 5)*

Explanation and modification:

As shown in Section 4.3, the manuscript proposes the following suitable monitoring methods referring to the plate-shaped translational landslide, such as long-period and multiple parameters monitoring, and additional monitoring suggestion is the inclination measuring device for plate girders, and this monitoring method in next working plan will be effective and suitable for this type of landslide.

In origin manuscript, the optimization monitoring methods may not be very clear, so we have highlighted the new method suggested in the next step of landslide monitoring, therefore, it is beneficial to in-depth exploration of the deformation and failure mode of the landslide and it will improve the success rate of early warning.

2. Reply to the reviewer 2# (professor Darve)

Dear professor Darve:

We are very grateful to receive your referee comments (RC) again. As you said in short comments (AC), this manuscript needs to be modified and improved in two main aspects, the first is to build the geomechanical model with more comments about the limits of the equilibrium method in Section 3.1, on the other hand is to add more details about my FEM modeling in Section 3.2. After careful discussion by author and co-authors, we found that these comments are very important for improving the quality of this manuscript.

With your help and comments, especially FEM computations with Mohr Coulomb criterion and FEM computations with the second order work criterion, we realized that the geomechanical model of landslide is relatively simple, which is a purely static method, and it ignores the influence of strain history. Moreover, in the numerical simulation calculation, the boundary conditions are set relatively simple, and the working conditions considered are also less than the actual situation. And we want to use the DEM to establish the landslide model in next research, and discuss the influence of pore water pressure on the sliding body sliding and soil damage, and compare it with the existing model. These shortcomings in this manuscript will be improved in future research.

Please see the detailed revision, and we carefully proof-read the manuscript to minimize typographical, grammatical, and bibliographical errors, and the modified parts are marked in red in the revised manuscript in supplement online.

Thank you very much for your suggestion and consideration, and we look forward to get your constructive advice.

Best regards,
Yimin Liu, Guiyun Gao and Chenghu Wang.

Detailed revision for comments of reviewer 2#

1. *To add in the paper some comments about the limits of the equilibrium method. (comment 1)*

Modification:

With the help of references about limit equilibrium method and instabilities in geomaterials, we add the following supplement in Section 3.1 from line 279 to 286.

According to characteristics of the Wobaoshi landslide in Section 1.2, when the geomechanical model is established, the cover layer is neglected, and the static geomechanical model of the plate-shaped rock sliding body is established based on the limit equilibrium method. The basic characteristic of the limit equilibrium method

is that the Mohr-Coulomb failure criterion of the soil in static equilibrium conditions is considered, that is, the problem's solution is solved by analyzing the destruction of the soil's balance. And soli elastic-perfectly plastic model was chosen, which obey the Mohr-Coulomb failure criterion and associated flow rules (Darve et al., 2004; Labuz et al., 2015).

2. *To give more details about your FEM modeling in the present state of your paper. (comment 2)*

Modification:

This comment is very important for the paper, and the FEM modeling is lack of detailed description, we add the following supplement in Section 3.2 from line 355 to 363.

The position of the right side of the landslide about 30m from the foot of the slope is selected as the right boundary of the model; the lower boundary is setted at the elevation of 0 m; the left boundary is located inside the mountain, about 30m away from the plate girder I. The element type adopts a plane strain quadrilateral-triangle mixing element, and the whole model is divided into 13775 elements and 14026 nodes. Here we constrain the vertical and horizontal displacement of its bottom boundary, and the left and right boundary conditions are set to constrain the horizontal displacement. The model uses steady-state seepage calculation, and the water levels at the left and right boundaries were set to 342 and 275 m, respectively. The typical pore-water-level data in the crack I and crack II presented in Table 3 were introduced into the finite element model, and were selected for a typical change period presented in Table 5.

Table 5 Loading steps of the water level in Crack I and II in FEM model

Loading Steps	Crack I	Crack II
0	314.50 m	311.00 m
1	316.00 m	313.00 m
2	317.50 m	315.00 m
3	316.00 m	313.00 m
4	314.50 m	311.00 m

3. *The paper chose a so low friction angle of 11.2 °for clay –what seems unrealistic. (comment 3)*

Modification:

It is very interesting for the value of friction angle, and it seems too low and unrealistic, so we add the explanation and discussion in Section 4.2 from line 445 to 453.

The internal friction angle, θ = 11.2 °, is so low for clay, which seems unrealistic. However, the angle θ is obtained by triaxial compression tests of the core, which is taken from the sand-mudstone contact surface in sliding surface, and the internal friction angle θ = 11.2 ° (Chen et al., 2015). One of the reasons may be that the clay layer is severely weathered, so its internal friction angle is small. In general, the

dilatancy effect obtained by the associated flow law is much larger than the actual observation, especially in the case of laternal infinite (Tschuchnigg et al., 2015a). However, for slope stability analysis, laternal infinite is not considered in most cases, and the dilatancy effect is not significant (Griffiths & Lane, 1999). Therefore, it is reasonable to set the dilatancy angle to be equal to the internal friction angle.

References：

Chen L., Liu Y., Feng X.: The investigation report on remediation project of Wobaoshi landslide, Sanhui Town, Enyang District, Bazhong City, The Institute of Exploration Technology of CAGS, Chengdu, Open File Rep., pp.57, 2015.

Darve F., Vardoulakis I.: Degradations and Instabilities in Geomaterials, Springer Vienna, Austria, 2004.

Griffiths, D. V., Lane, P. A.: Slope stability analysis by finite elements, Géotechnique, 49(3), 387-403, 1999.

Labuz J. F., Zang A.: Mohr–Coulomb Failure Criterion, Rock Mechanics and Rock Engineering, (2012)45:975–979, 2012.

Tschuchnigg, F., Schweiger, H.F. & Sloan, et al: Slope stability analysis by means of finite element limit analysis and finite element strength reduction techniques. Part I: Numerical studies considering non-associated plasticity, Computers and Geotechnics, 70, 169-177, 2015.

Tschuchnigg, F., Schweiger, H.F., Sloan, S.W., et al: Comparison of finite-element limit analysis and strength reduction techniques, Géotechnique, 65(4), 249-257, 2015.

Analysis of the instability conditions and failure mode of a special type of translational landslide using long-term monitoring data: A case study of the Wobaoshi landslide（in Bazhong，China）

Yimin Liu[a,b] , Chenghu Wang[a,*] , Guiyun Gao[a] , Pu Wang[a] , Zhengyang Hou[a] , Qisong Jiao[a]

[a] Institute of Crustal Dynamics, China Earthquake Administration, Beijing, 100085, China

[b] School of Manufacturing Science & Engineering, Sichuan University, Chengdu, 611730 ,*China*

Abstract: A translational landslide comprising nearly horizontal sandstone and mudstone interbed was widely developed in the Ba river basin of the Qinba–Longnan mountain area. Some progresses on the formation mechanism and failure mode for this type of rainfall-induced landslide have been made in the previous research; however, owing to lack of landslide monitoring data, it is very difficult to demonstrate and validate previously-established geomechanial model. This study considered a translational landslide with an unusual morphology: the Wobaoshi landslide, located in Bazhong city, China. Firstly, the engineering geological conditions of this landslide were ascertained through field investigation, and the deformation and failure mechanism of the plate-shaped sliding body were analyzed. Secondly, long-term monitoring engineering was conducted to obtain multi-parameter monitoring data, such as crack width, rainfall intensity, and pore-water pressure. Finally, based on the geomechanical model analysis of the multi-stage sliding bodies, the equation for the critical water height of the multi-stage plate girders, h_{cr}, was established, and the long-term monitoring data were used to verify its reliability. On the basis of numerical simulation and calculations, the deformation and failure modes of the plate-shaped sliding bodies were analyzed and investigatied. In conclusion,

the multi-parameter monitoring data proved that the stability of the sliding body is controlled greatly by the rainfall intensity and pore-water pressure and the pore-water pressure in the crack is positive for the initiation of the plate-shaped bodies sliding, and at the same time, one optimized monitoring methodology for this type of landslide was proposed. Therefore, this research findings are of theoretical and practical significance for the intensive study of translational landslides in this area.

Keywords: Translational landslide; Long- term monitoring; Instability conditions; Failure mode; Plate-shaped sliding body; Pore-water pressure.

0. Introduction

A special type of landslide occurs in the red beds of the Qinba–Longnan mountainous area. This landslide is mainly developed in the rock mass of the nearly horizontal sand and mudstone interbed in the Ba river basin, and it has the following characteristics: the cover layer is extremely thin, generally not more than 5 m; the sliding surface is close to horizontal; and the rock layer inclination angle is generally only 3° - 8°. The sliding body of this landslide is typically a thick layer of sandstone with good integrity, and its bottom is a weak layer comprising mudstone. During monsoon, particularly when rainstorms occur, the sliding body is pushed horizontally along the sliding surface. Some scholars call this phenomenon a flat-push landslide, which is a typical rainfall-induced landslide (Zhang et al., 1994; Fausto G. et al., 2004; Xu et al., 2010).

Research on the formation mechanism and deformation mode of a translational landslide is mainly based on two perspectives. The first category includes the translational landslides is primarily induced by the hydrostatic pressure or confined water pressure resulting from rainstorms

(Kong and Chen, 1989; Matjaž et al., 2004; Yin et al., 2005). The sliding body of the thick sandstone can slide along the surface because of the hybrid action of the hydrostatic pressure in cracks and the uplift force of the sliding surface (Wang et al., 1985; Zhang et al., 1994; Xu et al., 2006; Fan, 2007). Simultaneously, the sliding soil, expanded by rain water, causes a slip between nearly horizontal layers (Yin et al., 2005). The second category includes landslides wherein the hard rock layer covered by the upper layer (such as granite and sandstone) has a crushing effect on the lower weak rock layer, thereby causing the rock mass to laterally expand, resulting in a landslide (Cruden et al., 1996; Emelyanova, 1986).

Regarding the theoretical study on rainfall-induced translational landslide, scholars worldwide have used physical simulation experiments, gemechanical model analysis, and satellite remote-sensing methods to investigate the genetic mechanism, initiation criteria, and sensitive safety factors. Fan Xuanmei et al. (2008) reproduced the deformation and failure process of landslides through physical simulation, and further verified the formation mechanism and initiation criterion formula of the flat-push landslide previously studied by Zhang et al. (1994). Sergio et al. (2006) focused on the influence of pore-water pressure on the stability of rainfall-induced landslides, and studied the soil failure mode based on pore-water pressure via simulation experiment. Mario et al. (2008) and Teixeira et al. (2015) selected rainfall data from historical periodic rainfall conditions, and used physical experiments to establish an optimization model for rainfall-induced landslide initiation criteria for landslides in the southern Apennines and shallow landslides in northern Portugal; they also evaluated landslide susceptibility and safety factors to evaluate the possibility of landslide resurrection induced by rainstorms. Barlow et al. (2003) and Martin et al. (2005) used US land satellite called enhanced thematic mapper (ETM+)

and digital elevation model (DEM) data to detect the residues of translational bedrock landslides in an alpine terrain. Bellanova et al. (2018) used resistivity imaging to investigate the Montaguto translational landslide in the southern part of the Apennines; they also established a refined geometric model to observe the lithologic boundaries, structural features, and lateral and longitudinal discontinuities associated with sliding surfaces.

Through data collation and analysis of the current research status of translational landslides, scholars worldwide have conducted further research on the formation characteristics and genetic mechanism of translational landslides. Based on the results of previous studies, the main focus of this study is on the following two aspects.

(1) The occurrence of plate-shaped translational landslides is often unexpected and covert. Plate-shaped translational landslides are primarily induced by rainfall; such events often occur in the red-bed zone of the Qinba–Longnan mountainous area. Due to the dense population and infrastructures in this area, plate-shaped landslides, characterized by large volumes, and covert and abrupt occurrence, often cause massive property loss and casualties. In the previous field investigation, such destructive events are often classified as small-scale rock mass collapses; hence, the dangers posed by such kind of landslides were easily ignored.

(2) The field investigation and monitoring data for this kind of landslide is often absent. In the past research, specific geomechanical and physical models have been established using historical rainfall records, and laboratory physical experiments have been conducted in the to verify the failure model. However, long-term on-site monitoring data and related analysis and findings for such landslides have not been reported in publications according to literature review. Therefore, several key field monitoring parameters, such as width of rear crack, real-time rainfall,

pore-water pressure, and groundwater level, should be abtained to investigate and validate the deformation and failure mode of translational landslides, and be utilized to establish a geomechanical model.

Based on the formation mechanism of the translational landslide established by previous studies, research chosen a typical and specific translational landslide (the Wobaoshi landslide) in the Ba River Basin of the Qinba–Longnan mountainous area, and conducted field investigation, long-term (February 2015 to July 2018) monitoring, geomechanical model analysis, and numerical simulation to investigate the instability conditions and variation failure modes of this translational landslide under the influence of periodic rainfalls.

1. Enginereing Geology Characteristics of the Wobaoshi Landslide

1.1. Field Survey of the Landslide

The Wobaoshi landslide is located in the Ba river basin in the Qinba–Longnan mountainous area. Its specific location is in Baiyanwan village, Sanhui town, Enyang district in Bazhong, China. Fig. 1 presents its geographical location and elevation information. The Wobaoshi landslide is located on the left bank of the Shilong river. The front edge of this landslide is in the curved section of the river, and its left boundary gully is located on the concave bank on the river's left bank. The landslide area is classified as a red-bed layer in a low mountainous area, the vegetation of its sliding body is dense, and its geomorphic unit is cuesta structural slope. The geological structure of the landslide body lies on in the south side of the Nanyangchang anticline, and its stratum is the mudstone and sandstone interbed of the Penglaizhen Formation of the upper Jurassic series (Chen et al., 2015).

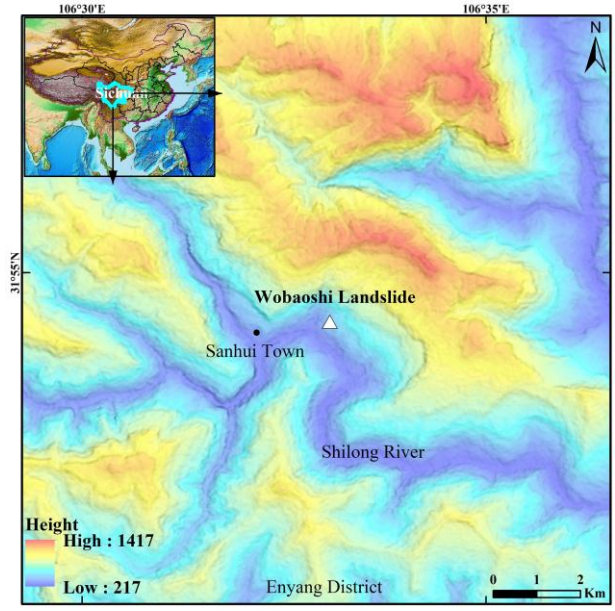

Fig. 1 Geographical location and elevation map of the Wobaoshi landslide.

This landslide is common in the eastern subtropical monsoon climate region, where rainfall is abundant and mostly concentrated from May to October, accounting for 75% - 85% of the total annual rainfall. The monthly average rainfall is above 100 mm, of which the highest occurs in July, the monthly average rainfall in July is over 200 mm and often accompanied by rainstorms, and the rainfall gradually decreases after August in this region (Chen et al., 2015). The types of groundwater are mainly fissure water in weathered bedrock and pore-water in trailing edge cracks, and the dynamic change of groundwater is considerably affected by climatic change.

1.2. Landslide Characteristics and Forming Conditions

1.2.1 Enginereing Geology Characteristics

According to the satellite remote-sensing interpretation and landslide survey, the shape of the sliding body is a flat long rectangle on the plane. Its longitudinal (sliding) direction is nearly 32 m, the lateral width is 160 m, the average thickness of the sliding body is approximately 30 m, and its volume is approximately 1.536 × 105 m^3. This sliding body belongs to small- to medium-sized landslides according to the typical scale. The sliding direction of the landslide is 249°, and the overall attitude of the rockbed is 170° - 180° ∠6° - 8°. The strike in this landslide is nearly parallel to the overall trend of the bank slope, which is a typical nearly horizontal consequent bedding rock slope. Fig.2 shows a planar graph of the Wobaoshi landslide and photographs of five observation points. Fig. 3 presents I-I′ sectional graph of the landslide.

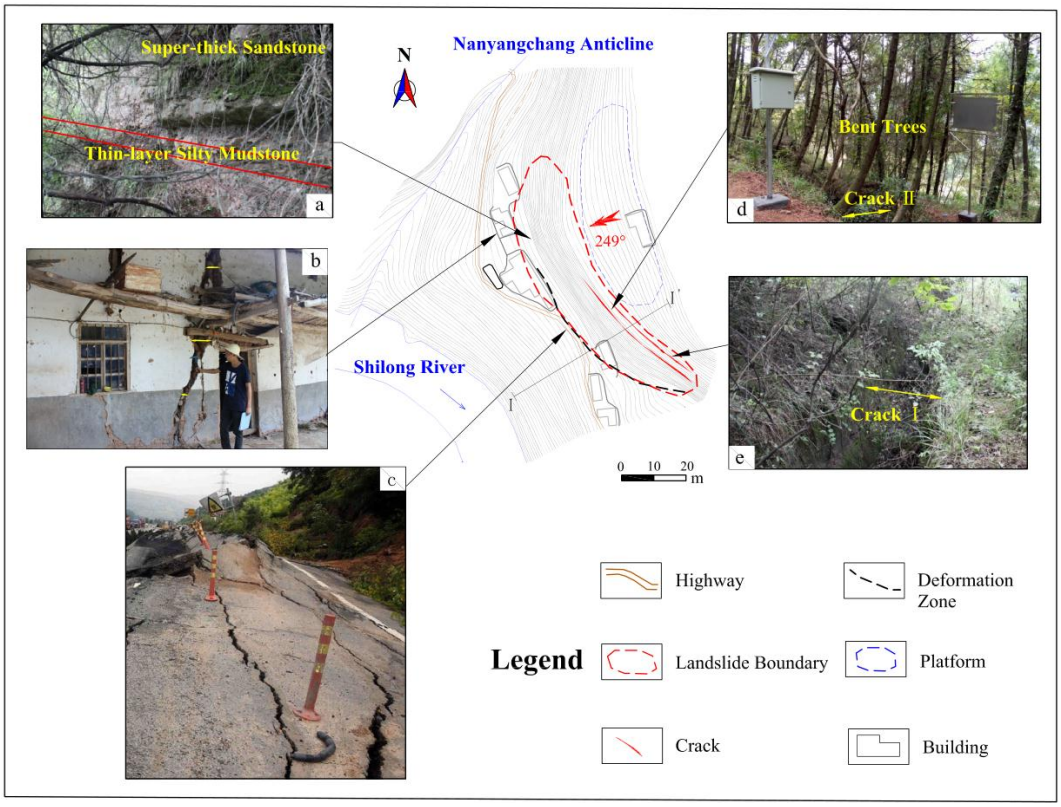

Fig. 2 Topographic map of the Wobaoshi landslide and photographs of observation points: (a) exposed bedrock at the front edge; (b) the houses had cracked at the front edge (c) the roadbed is pushed uplifted at the front edge; (d) crack II and bent trees; and (e) crack I.

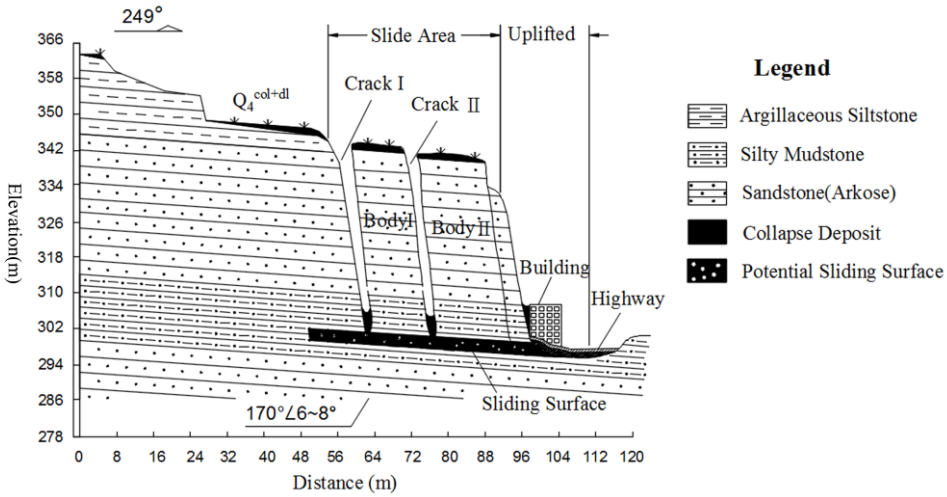

Fig. 3 I-I' sectional graph of the landslide

As shown in Fig. 2, the landslide shape is special, the longitudinal length is much less than the lateral width and is even smaller than the thickness of the sliding body. Therefore, this body can be easily mistaken for a multistage dangerous rock mass with dumping deformation during disaster investigation. According to Fig. 3, the inclination of the landslide is almost erect, and a

147 group of long and straight structural planes parallel to the slope cut the slope into two thin plates
148 (sliding bodies I and II); furthermore, the surface structure of the slope has a certain degree of
149 aperture, both sides of the crack are closed, and the bottom of the crack is filled with clay in
150 addition to gravel and collapse deposits.

151 1.2.2 Forming Conditions

152 The sliding body of the Wobaoshi landslide formed two obvious cracks from the outside to
153 the inside, which cut and disintegrated the sliding body into plate-shaped blocks from front to
154 back, as shown in the photographs of observation points c and d in Fig. 2. Then, the plate-shaped
155 sliding bodies I and II were formed. The landslide is a two-stage translational landslide in which
156 the longitudinal length of sliding body I is 12 m, the identifiable lateral width is ~ 70 m and the
157 thickness is ~ 30 m, the longitudinal length of the sliding body II is 16 m, the identifiable lateral
158 width is ~ 65 m, and the thickness is ~ 28 m. Sliding body I forms crack I with the trailing edge of
159 the landslide, and sliding body II forms crack II with sliding body I. When large rainfall intensity
160 occurs during monsoon, the pore-water in the cracks can be observed, thus indicating that cracks I
161 and II have preferable water-storage conditions.

162 As the photograph of observation point d in Fig. 2 shows, bent trees grow on the trailing edge
163 of landslide bodies I and II. The trees on the landslide are skewed with the soil mass sliding, and
164 after the sliding stops, the upper part of the trunk turns to the upright state year by year. The
165 existence of bent trees represents the tendency of the slope body to become unstable or the
166 existing landslide accumulation body tends to slide again, this is also historical evidence of the
167 slow sliding of the landslide (Zhang Lizhan et al., 2015).

168 As the photo of observation point a in Fig. 2 shows, the shallow surface of the Wobaoshi
169 landslide is a 2–3 m thick layer of collapsed and plowed soil. The sliding body contains extremely
170 thick sandstone with good integrity, and the bottom sliding surface is a weak interlayer comprising
171 of silty mudstone. In summary, the Wobaoshi landslide is a typical and special translational
172 landslide, and based on the characteristics of its plate-shaped body, it can be considered a
173 plate-shaped landslide (Fan et al., 2008; Xu et al., 2009).

174 The engineering geological conditions of the Wobaoshi landslide are inferred on the basis of
175 its characteristics; i.e., the rapid immersion of groundwater softens the joint surface of soil and

rock formation, especially under a rainstorm. Then, the group of open cracks parallel to the slope in the sliding body is concentrated and quickly filled with water, following which groundwater level rises and the pore-water pressure increases sharply, such that the sliding bodies I and II slide horizontally along the contact surface of the bottom sand-mud-rock weak layer. This condition changes the stress mode and equilibrium state of the rock and soil mass, thereby easily inducing a landslide. As shown observation point b and c in Fig. 2, the Wobaoshi landslide seriously threaten residential houses and highways, the houses had cracked and highways had uplifted on its front edge, so this landslides seriously threatens the safety of people's property and transportation.

2. Landslide Monitoring Scheme and Monitoring Data Analysis

2.1. Long-term Monitoring Scheme

According to the detailed investigation of the Wobaoshi landslide, two cracks extend through the sliding surface at the trailing edge of the landslide, and the pore-water in the cracks exists during periodic rainfalls. As the hydrostatic pressure in the cracks strongly influences the stability of the plate-shaped landslide (Fan Xuanmei et al., 2008; Guo Xiaoguang et al., 2013), via real-time monitoring of cracks, rainfall and pore-water pressure measurements were conducted from February 2015 to July 2018 to determine the landslide state in different periods such as rainy and non-rainy seasons, together with the interaction between multilevel plate girders and sliding surface. Fig.4 shows the layout graph of the monitoring equipment.

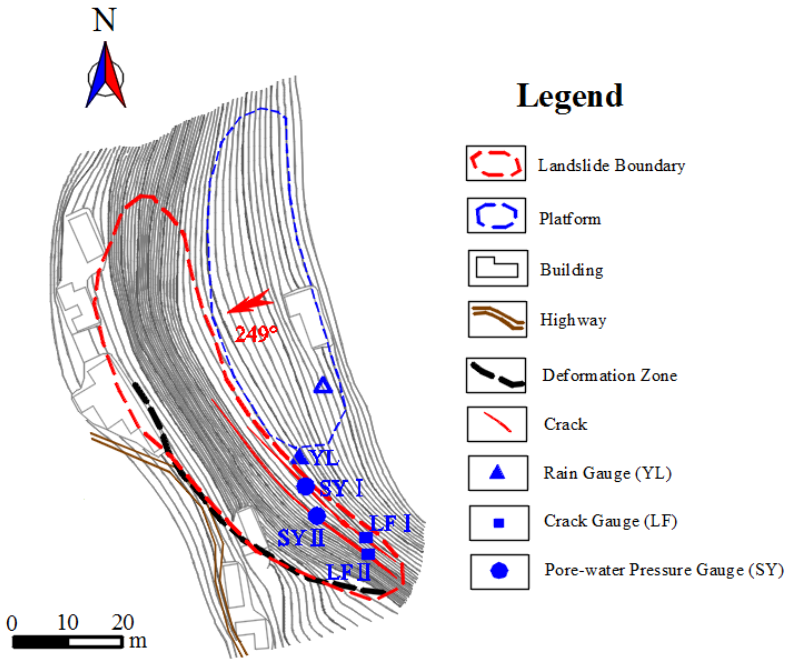

Fig. 4 Layout planar graph of the monitoring equipment

As shown in Fig. 4 shows, two non-contact crack automatic monitors, LF I and II, are installed on both sides of cracks I and II, respectively, to record real-time variation of the width of the two cracks (Yimin Liu et al., 2015). An automatic rain gauge is installed in flat space and no tree occlusion is observed at the trailing edge of the landslide to record real-time and cumulative values of the rainfall. Two pore-water pressure gauges are installed at the bottom of crack I and II to measure the pore-water pressure. The value of pore-water level, h_c, can be calculated using the relation $h_c = H - h_i + hs$, where *hi* is the installation depth of the pore-water pressure gauge; H is the depth of the crack; and h_m is the measured value of the pore-water pressure gauge.

In this example, the initial width value of crack I is 5.640 m, and the initial width value of crack II is 4.492 m (the first measurement was conducted in January 2015); the installation depth h_{i1} = 24.72 m, and the depth of crack I is H_1 = 38 m, with h_{c1} = 13.28m + h_{m1}. Additionally, the installation depth h_{i2} = 24.85 m, and the depth of crack I is H_2 = 35 m, and h_{c2} = 10.15m + h_{m2}. The monitoring frequency of the crack width is thrice a day, the monitoring frequency of the pore-water pressure is twice a day, and the rainfall intensity adopts the accumulative value of one month. The multiparameter monitoring data are transmitted to the monitoring server through the GPRS network.

(a) (b) (c)

Fig. 5 Photos of monitoring instrument installation: (a) crack I gauge; (b) rain gauge and pore-water pressure gauge; (c) crack II gauge.

2.2. Monitoring Data Analysis

By the monitoring work performed on the Wobaoshi landslide for three-and-a-half years (February 2015 to July 2018), this study selected the typical data of the width of cracks I and II, the pore-water pressure and the rainfall intensity, details of these monitoring data are in listed in Tables 1 and 2. The corresponding time curves in Fig.6 show the monitoring data of the rainfall intensity and the width of cracks I and II. Fig.7(a) and 7(b) present comparison curves of the monitoring width data of cracks I and II against their pore-water pressures, respectively.

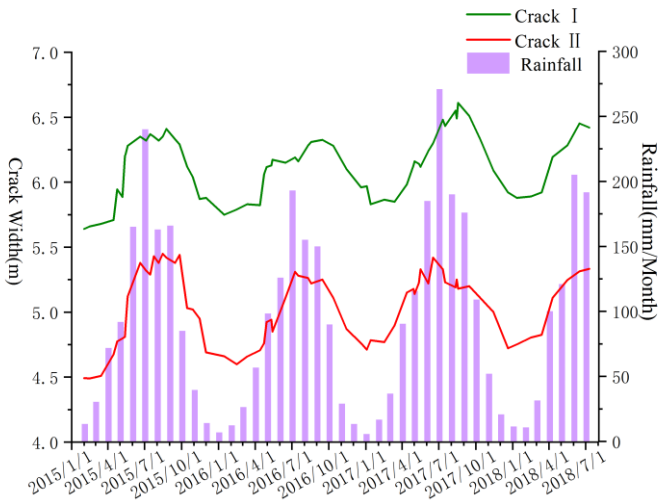

Fig. 6 Monitoring data curves (rainfall intensity and width of cracks I and II)

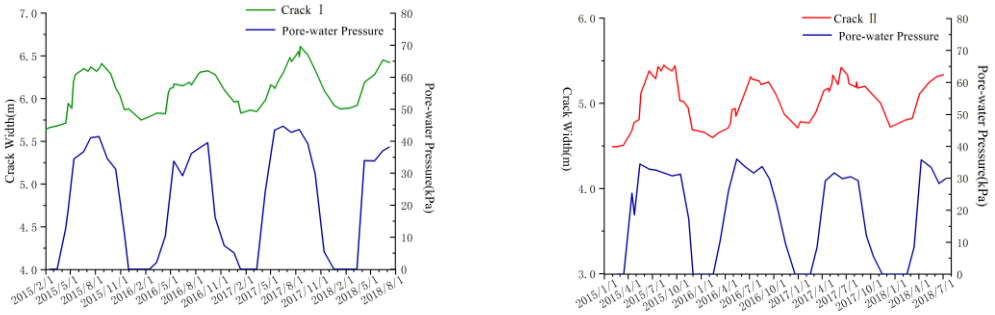

(a) (b)

Fig. 7 Monitoring data curves: (a) width of crack I and its pore-water pressure; (b) width of crack II and its pore-water pressure.

Based on the comprehensive comparison and analysis of the data curves presented in Figs. 6 and 7, this study concludes that the Wobaoshi landslide is still in creep deformation state, and the plate-shaped sliding body exhibits a regular trend with changes in rainfall intensity and pore-water pressure. Cracks I and II show a preferable water-storage capacity during monsoon, and increasing pore-water pressure affects the crack width variation. The specific analysis is as follows.

(1) A clear correspondence exits between the absolute amount of crack width change and season change (i.e. change in rainfall intensity); the magnitude of the rainfall intensity determines the change of the width of the two cracks. As shown in Fig. 6, the widths of cracks I and II widen as the rainfall intensity increases during monsoon (May to September), and their crack widths gradually decrease as the rainfall intensity lowers during the non-rainy seasons (October to April in the next year). As indicated in Fig. 8, the maximum width of crack I reaches 6.615 m, and the absolute stretching amount of this crack is close to 1 m in the July–August period in 2017 (monthly rainfall exceeding 250 mm). The maximum width of crack II is also in the range of 5.40–5.45 m, and its absolute stretching amount exceeded 1 m during July–August 2015 and

July–August 2017. During non-rainy seasons, when the rainfall intensity lowers, the crack width begins shrinking, and it decreases to its minimum in January in each monitored year.

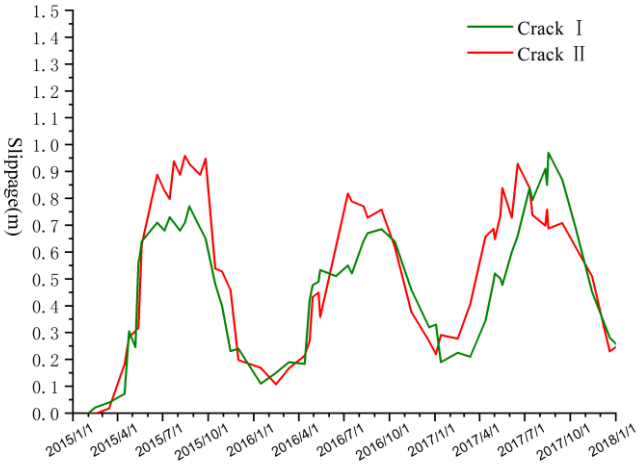

Fig. 8 Absolute slippage amount curves of crack I and II

(2) The width of cracks I and II tend to increase year by year, indicating that the two-stage sliding body of the Wobaoshi landslide is still moving along the sliding surface because of the influence of rainfall. In Fig. 6, the measured data in the monitoring period indicate that the minimum widths of crack I and II are gradually increasing, and their maximum value is considerably affected by the rainfall intensity of a particular month.

(3) Fig.7 shows that the stretching of cracks I and II, or both follows the same trend as the pore-water pressure, i.e., the magnitude of pore-water pressure determines the width variation of the cracks. Fig.7 also shows that the water-storage capacity of crack I is good during monsoon, and after the sliding body slides, it can maintain a certain pore-water level because of rainfall replenishment. Additionally, the increase in rainfall intensity increases the water level in the cracks, and the increase in pore-water pressure positively affects the initiation of the plate girder.

The curve in Fig. 8 shows that the increase in pore-water pressure has a significant causal relationship with the stretching of the cracks.

3. Model Calculation and Numerical Simulation

To construct a generic model of the evolution process of the Wobaoshi landslide, a geomechanical model of plate-shaped sliding bodies was established, its stability was calculated，and it was combined with monitoring data for a comparative analysis. According to previous findings(Fan, 2007; Fan et al., 2008; Xu et al., 2010), when many penetrating cracks are parallel to the slope in the rock mass, and these cracks are filled with water, the water pressure on both sides of each plate-shaped body attains in a balanced state except for the outermost body. However, once the outer body slides, owing to the sudden decrease of the pore-water level in the trailing edge crack, the water pressure around immediately following plate-shaped body becomes unbalanced, and new sliding damage is induced (Fan, 2007; Xu, 2008).

3.1. Model Establishment and Stability Calculation

According to characteristics of the Wobaoshi landslide in Section 1.2, when the geomechanical model is established, the cover layer is neglected, and the static geomechanical model of the plate-shaped rock sliding body is established based on the limit equilibrium method. The basic characteristic of the limit equilibrium method is that the Mohr-Coulomb failure criterion of the soil in static equilibrium conditions is considered, that is, the problem's solution is solved by analyzing the destruction of the soil's balance. And soli elastic-perfectly plastic model was chosen, which obey the Mohr-Coulomb failure criterion and associated flow rules (Darve et al., 2004; Labuz et al., 2015).

For the failure mode of the two-stage plate girders of the Wobaoshi landslide, this study selected a typical section of plate-shaped sliding bodies and established the geomechanical model, shown in Fig. 9. In this section, first, a stability analysis of the outer layer plate girder II, is conducted and then the inner plate girder I is analyzed.

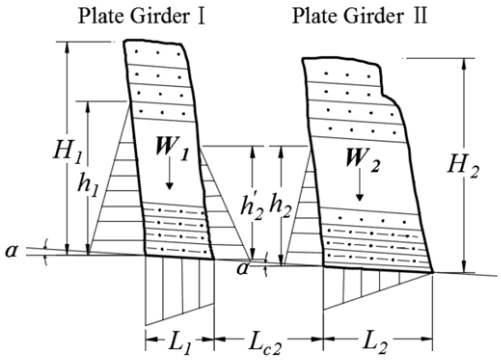

Fig. 9 Geomechanical model of two-stage plate-shaped sliding bodies

In Fig. 9, α is the angle of the sliding surface, h_1 and h_2 are the heights of the pore-water levels in cracks I and II, respectively; L_1 and L_2 are the widths of plate girders I and II, respectively; L_{c2} is the distance between plate girder I and II; H_1 and H_2 are the heights of plate girders I and II; respectively, and W_1 and W_2 are the self-weights of plate girders I and II per unit width, respectively. According to the relationship between the stability coefficient of plate girder, K, and the height of the pore-water level, h, shown in Fig. 8 (Zhang et al., 1994; Xu et al., 2010), while considering the internal cohesive force of the sliding surface, the equation to calculate the stability coefficient, K_2, of the outer layer plate girder II is expressed as follows:

$$K_2 = \frac{\left(W_2 \cos\alpha - \frac{1}{2}\gamma_w h_2 L_2 - \frac{1}{2}\gamma_w h_2^2 \sin\alpha\right)\tan\theta + cL_2}{\frac{1}{2}\gamma_w h_2^2 \cos\alpha + W_2 \sin\alpha}. \quad (1)$$

In Eq. (1), c is the internal cohesion of the sliding surface; γ_r is the saturated gravity of the sandstone; γ_w is the gravity of water; and $W = H \cdot L \cdot \gamma_r$. K_2 is set to 1, i.e., the plate girder II is set in a critical sliding state (GB/T 32864-2016, 2017). Then Eq. (2) of the maximum pore-water level of plate girder II, h_{cr2}, is derived from Eq. (1).

$$h_{cr2} \approx \frac{1}{2\cos\alpha}\left[L_2^2\tan^2\theta + \frac{8}{\gamma_w}\left(W_2\cos\alpha\tan\theta - W_2\sin\alpha + cL_2\right)\cos\alpha\right]^{\frac{1}{2}} - \frac{L_2}{2\cos\alpha}\tan\theta \quad (2)$$

According to the experimental data of the triaxial confining pressure of the Wobaoshi landslide's rock core (Chen et al., 2015), the internal friction angle of the sliding surface is θ = 11.2 °, the saturated gravity of the sandstone is γ_r = 19.2 kN/m^3, the gravity of clear water is γ_w = 9.8 kN/m^3, and the internal cohesion of the sliding surface is c = 10.2 kPa. According to the sectional graph of the Wobaoshi landslide (see Fig. 2), H = 35 m, L = 16 m, and α = 6 °. Therefore, according to Eq. (2), h_{cr2} = 13.896 m.

Based on the stability analysis of plate girder II, combined with Eq. (1), Eq. (2), and Fig. 7, the equation to calculate the stability coefficient K_1 of the inner layer plate girder I can be expressed as Eq. (3). In addition, $h_2^{'} = h_2 - L_{c2}\,sin\alpha$ and L_{c2} = 3.8 m; therefore, $h_2^{'}$ = 13.499 m.

$$K_1 = \frac{\left[W_1\cos\alpha - \frac{1}{2}\gamma_w\left(h_1+h_2^{'}\right)L_1 - \frac{1}{2}\gamma_w\left(h_1^2 - h_2^{'2}\right)\sin\alpha\right]\tan\theta + cL_1}{\frac{1}{2}\gamma_w\left(h_1^2 - h_2^{'2}\right)\cos\alpha + W_1\sin\alpha} \quad (3)$$

Similarly, K_1 is set to 1 and, in plate girder I, H_1 = 38m, L_1 = 12m, α = 6 °, $h_2^{'}$ = 13.499m, therefore, the maximum pore-water level h_{cr1} of plate girder I can be calculated using the Eq. (3) and h_{cr1} = 17.249m.

The preceding calculation results show that, when the pore-water level at the trailing edge of the plate girder reaches the maximum height at which the landslide begins, i.e., when h_{cr1} = 17.249m and h_{cr2} = 13.896m, the pore-water pressure triggers the plate-shaped sliding bodies. In next section, the pore-water monitoring data, which were acquired via the landslide monitoring are

used to verify the equation.

The pore-water monitoring data in Section 2.2, which were acquired via the landslide monitoring engineering, were used to test the equation for calculating the maximum height of multistage plate girders, h_{cr}. According to the monitoring data of the pore-water pressure and the installation depth of the sensors, the actual calculated maximum height values h_{c1} and h_{c2} of the pore-water level are presented in attached Table 3. Combined with the change in the absolute stretching amount in Fig. 8, typical data of the measured pore-water level are selected, corresponding to the sudden change in the absolute slippage (see Table 3 for details), as shown in Fig.10.

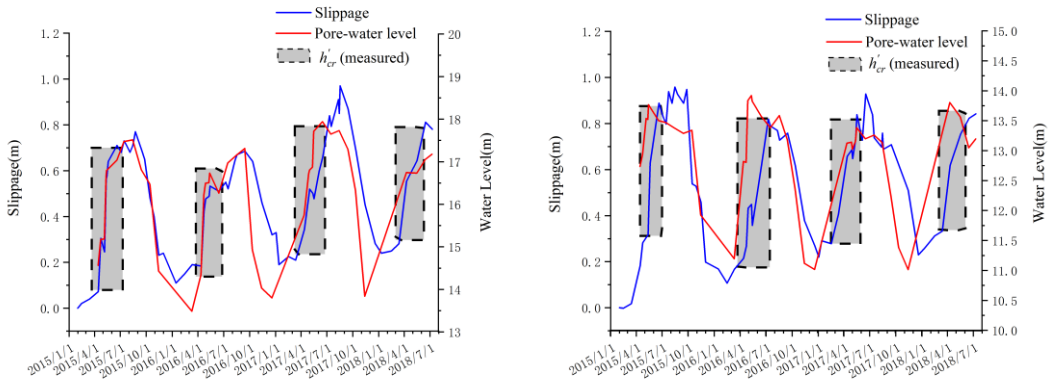

(a) Crack I (b) Crack II

Fig. 10 Determination of the maximum measured pore-water level $h_{cr}^{'}$

The dotted boxes in Fig. 10 represent the value of the pore-water level when the bodies are sliding, i.e., the maximum pore-water level, $h_{cr}^{'}$, which causes the sliding body to be unstable. The measured $h_{cr}^{'}$ in Fig. 10 can be compared to the relationship between the pore-water level, h, and the stability coefficient of the plate girder, K, in equation (1) and (3), which are also shown in Fig. 10.

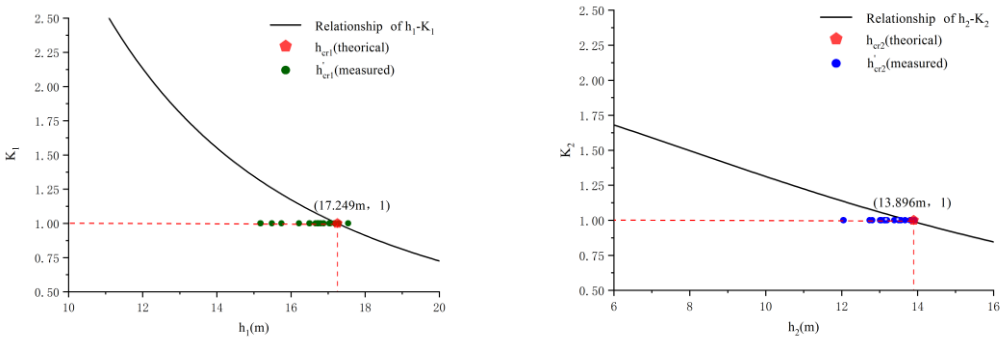

(a) Crack I (b) Crack II

Fig. 11 Comparison of $h_{cr}^{'}$(measured) and h_{cr} (theoretical)

In Fig. 11, the curves of the h-k relationship represent equations (1) and (3). The frequency of $h_{cr}^{'}$(measured) in Fig. 11 shows that most of the monitoring pore-water levels are not higher than those theoretically calculated. The Wobaoshi landslide monitoring example shows that in most cases, when $h_{cr}^{'}$(measured) $\leqslant$ h_{cr} (theoretical), the pore-water pressure causes the instability of the sliding body.

3.2. Numerical Simulation of the Plate-shaped Sliding Bodies

The numerical simulations and calculations of the plate girder were performed using MIDAS GTS NX geotechnical finite element software. First, the 1:1 sliding body model in Fig. 9 was introduced into the finite element software, and the mechanical parameters of the sliding body model, i.e., elastic modulus, Poisson's ratio, gravity internal cohesion and friction angel, were defined as shown in Table 4. The position of the right side of the landslide about 30m from the foot of the slope is selected as the right boundary of the model; the lower boundary is setted at the elevation of 0 m; the left boundary is located inside the mountain, about 30m away from the plate girder I. The element type adopts a plane strain quadrilateral-triangle mixing element, and the whole model is divided into 13775 elements and 14026 nodes. Here we constrain the vertical and horizontal displacement of its bottom boundary, and the left and right boundary conditions are set

to constrain the horizontal displacement. The model uses steady-state seepage calculation, and the water levels at the left and right boundaries were set to 342 and 275 m, respectively. The boundary conditions are set as follows.

(1) For the displacement boundary, the left and right boundaries constrained the displacement in the X-direction; i.e., TX = 0. For the bottom boundary, the displacement in the X and Y directions was constrained; i.e., TX = TY = 0.

(2) For the seepage conditions, the water levels at the left and right boundaries were set to 342 and 275 m, respectively.

The typical pore-water-level data in the crack I and crack II presented in Table 3 were introduced into the finite element model, and were selected for a typical change period presented in Table 5, followed by numerical calculations to obtain the typical deformation and displacement states of plate-shaped sliding bodies in the rainy and non-rainy seasons, as shown in Fig. 12.

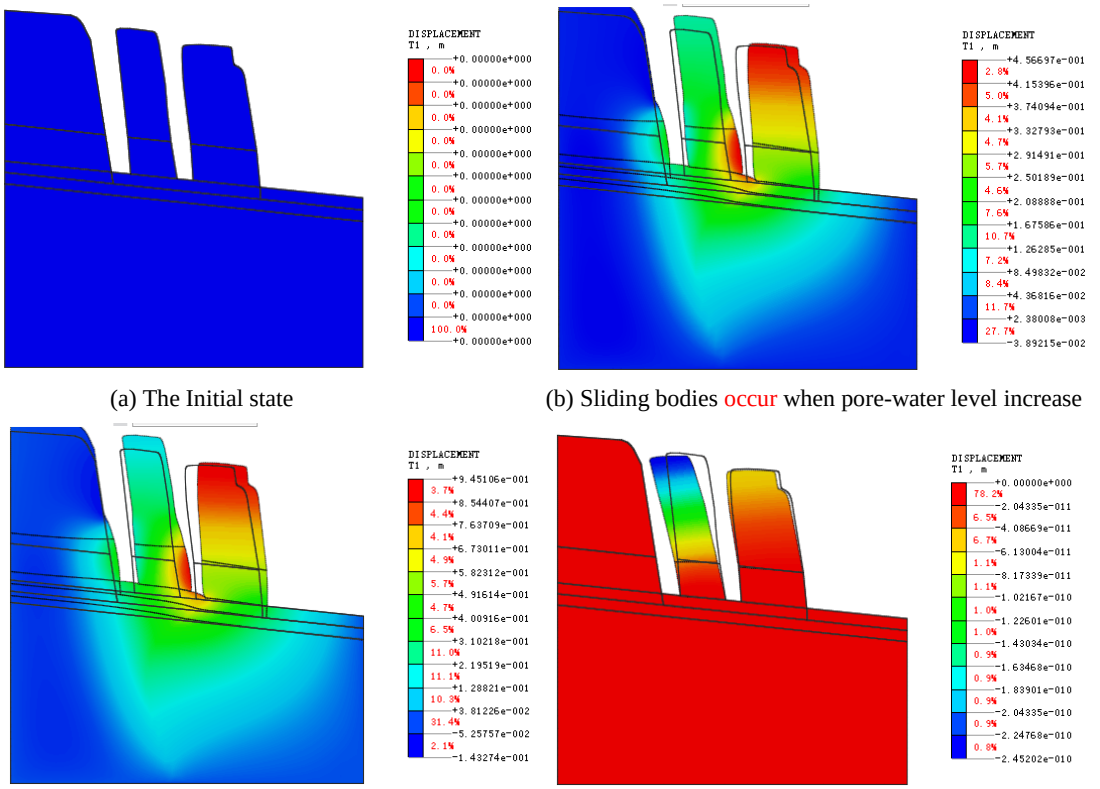

(a) The Initial state (b) Sliding bodies occur when pore-water level increase

(c) The sliding bodies slide to the maximum state (d) Sliding bodies tilt backward when water level decreases

Fig. 12 Example of finite element simulation and numerical calculation

The initial displacement state in Fig. 12(a) is set to zero for the following analysis. Figure

12(b) shows that, under the combined effect of the pore-water pressure and seepage, the multistage plate girders slide horizontally along the sliding surface. In Fig. 12(c), the multistage plate girders have slid to the maximum distance, where the maximum distance of slider II is 0.945 m, which is close to the value obtained in the monitoring data. In Fig. 12(d), owing to the decrease in pore-water level in the non-rainy season, sliding bodies I and II have the same tendency to tilt backward. Therefore, the calculation results of the numerical simulation can corroborate the sliding-body mechanics model and the landslide monitoring data.

4. Discussion

As mentioned in the previous sections, this special type of translational landslide, which has a plate-shaped sliding body and is generally formed in an extremely thick sandstone slope with a thin cover layer, is nearly horizontal and has good integrity. According to the traditional theory of granular equilibrium limit, deformation or sliding movement of this nearly horizontal bedrock slope is nearly impossible, and the likelihood of forming a landslide is minimal. However, this special structure of translational landslide widely occurs in the Qinba–Longnan mountainous area during the investigation of geological hazard hidden dangers. Therefore, in the investigation and risk assessment of geological hazards, the characteristics of the plate-shaped landslide and the deformation and failure mode should be combined to detect the hidden dangers with the geological conditions of the landslide. Combining the results of previous studies with those of the monitoring, the discussion herein is divided in the following three parts.

4.1. Deformation and Failure Mode Exploration of the Wobaoshi Landslide

The monitoring results of the Wobaoshi landslide in this case validate the rainfall-triggered failure mode of the translational landslide (Zhang Zhuoyuan et al., 1994). According to the landslide monitoring data, particularly the change trend of the cracks opening and closing in Section 2.2, and the numerical simulations of the plate-shaped sliding bodies in Section 3.2, the

deformation and failure mode of the landslide were obtained, as shown in Fig. 13. Fig. 13 shows the deformation of the plate-shaped sliding bodies in the Wobaoshi landslide during the monitoring period (non-rainy season–rainy season–non-rainy season). As shown in Fig. 13(b), the large amount of rainfall in monsoon causes the cracks to be filled with water; when the pore-water level reaches the maximum height at which the landslide begins, the increased pore-water pressure positively affects the initiation of the plate-shaped sliding body (Fan Xuanmei et al., 2007). When the pore-water pressure rises to the threshold value, the plate-shaped landslide can be triggered. In this monitoring case, the pore-water pressure can push the plate-shaped sliding body by nearly 1 m, resulting in the uplift of residential houses and highways on its leading edge. Therefore, we can infer that one or more penetrating cracks are likely parallel to the slope in the landslide body. With the approach of the rainy season, the plate-shaped sliding body II begins to slide first and the water pressure balance in the cracks is destabilized. This condition causes the gliding of the plate-shaped sliding body I, thus forming a multistage translational landslide with characteristic step-by-step backward movement.

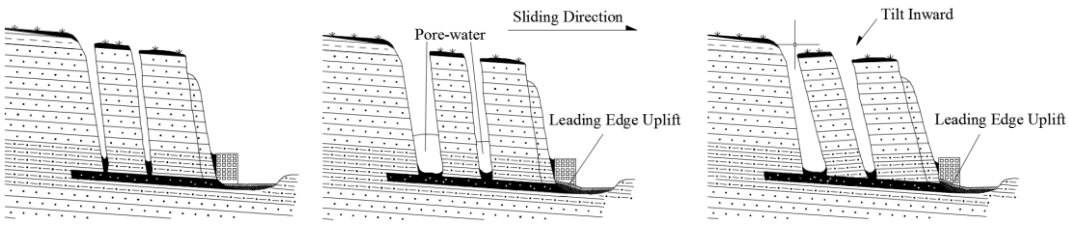

(a) Initial State of Plate Girder (b) Sliding in Rainy Season (c) Tilting in Dry Season

Fig. 13 Schematic of deformation and failure mode of the Wobaoshi landslide

As shown in Fig. 13(c), the plate girder is tilted to the trailing edge by the lower pore-water level and its own weight with less rain during the non-rainy season, thereby causing the plate girder to fall backward (inside the slope) until the top of the plate girder is in contact with the slope surface, the crack width begins shrinking, and a narrow A-shaped crack is formed. Monitoring data of the Wobaoshi landslide and numerical simulation of plate-shaped sliding body also verify the deformation and failure mode of the plate-shaped landslide post landslide occurrence (Xu et al., 2010). Year after year, the cracks at the bottom of the slab-shaped sliding body grow larger, and the degree of inclination of the plate girder continues to increase. The

434 degree of arching of the front edge also increases, which causes the stability of the landslide to
435 decrease continuously, thereby posing a high risk for the houses and roads on the front edge of the
436 landslide.

437 ## 4.2. Determination of Maximum Pore-water Level h_{cr}

438 The theoretical analysis and stability calculation of the geomechanical model of the plate
439 girder is described in Section 4.1, together with the initiation criterion for multistage sliding
440 bodies of translational landslide, i.e., determination of the maximum water height in the crack, h_{cr},
441 (Zhang et al., 1994) and calculation of the sliding body's stability coefficient, K, (Xu et al., 2010),
442 which is determined by the theoretical calculation of strata inclination, shape, weight, and physical
443 properties (such as saturated gravity, γ_r, internal cohesion of the sliding surface, c, and internal
444 friction angle of the sliding surface, θ) based on the limit equilibrium theory (Lin et al., 2010).
445 Therefore, the stability coefficient of the landslide exponentially decreases with the increase in the
446 water-filling height of the trailing edge crack (Fan, 2008; Xu et al., 2010).

447 The internal friction angle, $\theta = 11.2°$, is so low for clay, which seems unrealistic. However,
448 the angle θ is obtained by triaxial compression tests of the core, which is taken from the
449 sand-mudstone contact surface in sliding surface, and the internal friction angle $\theta = 11.2°$ (Chen et
450 al., 2015). One of the reasons may be that the clay layer is severely weathered, so its internal
451 friction angle is small. In general, the dilatancy effect obtained by the associated flow law is much
452 larger than the actual observation, especially in the case of laternal infinite (Tschuchnigg et al.,
453 2015a). However, for slope stability analysis, laternal infinite is not considered in most cases, and
454 the dilatancy effect is not significant (Griffiths & Lane, 1999). Therefore, it is reasonable to set the
455 dilatancy angle to be equal to the internal friction angle.

456 In this case, in the equation for calculating the maximum pore-water level, h_{cr}, deduced in
457 Section 3.1, comparing the measured data of the Wobaoshi landslide in Section 2.2, we can
458 observe that the measured maximum pore-water level, h_{cr}', is close to the theoretical maximum
459 pore-water level, h_{cr}, thus validating the calculation equation of h_{cr}, and the instability conditions
460 of the sliding bodies. Additionally, the most measured data in Tab. 3 are slightly smaller than the

theoretical calculation value, i.e., $h_{cr}^{'} \leq h_{cr}$. Thus, compared with the calculation equation of the maximum water height proposed by Zhang et al. (1994) and the physical simulation experiment conducted by Fan et al. (2008), the monitoring case of the Wobaoshi landslide shows that the measured data $h_{cr}^{'}$ is mostly lower than the theoretical calculated value, h_{cr}, which can cause instability of the sliding body. The reason for this instability may be that the actual cohesion value c' of the sand-shale contact surface is smaller than the cohesive force value c of the sliding surface in equation (2) during the creep state of the landslide for a long duration or that the frictional angle of the sliding surface, θ, changes slightly. According to the calculation of the stability coefficient, K, in equation (2), when $c' \leq c$, $h_{cr}^{'} \leq h_{cr}$ is obtained, the plate girder slides in the case wherein $h_{cr}^{'}$ (measured) is not larger than h_{cr} (theoretical).

4.3. Optimization Methods of Landslide Monitoring

Focusing on the plate-shaped translational landslide through the existing field monitoring result experience and deformation and failure mode exploration, this study proposes the long- term monitoring method with more parameters referring to the characteristics of suchlandslides.

First, long- term monitoring should be conducted to obtain sufficient monitoring data, which mainly includes obtaining groundwater level, pore-water pressure, rainfall intensity, and displacement data on the front edge of the landslide during monsoon, as well as focusing on the change of overall inclination of the plate girder during the non-rainy season. This is because the inclination angle α relative to the sliding surface also changes after the sliding of the plate girder. Thus, the inclination measuring device which consists of three-axis accelerometer and electronic compass should be installed in the sliding body, to verify the theoretical exploration of deformation mode of the plate-shaped sliding body in the non-rainy season in Fig. 13(c). Furthermore, a sensitivity analysis of various parameters affecting the stability coefficient K of the sliding body (such as the pore-water level, internal cohesive force in saturated water, internal

485 friction angle of the sliding surface, and inclination angle of the plate girder) should be conducted
486 on the basis of the monitoring data. Therefore, an in-depth analysis and exploration of the
487 deformation and failure mode of the plate-shaped landslide would be beneficial and would
488 improve the success rate of landslide warning.
489

490 # 5. Conclusions

491 Considering the case of the Wobaoshi landslide as an example, this study uses research
492 methods such as field exploration, a long- term monitoring engineering, geomechanical model
493 analysis and numerical simulation to deeply analyze the instability conditions and failure
494 characteristics of a special type of translational landslide. The research results are beneficial to the
495 stability analysis and evaluation of this type of landslide. Targeted monitoring methods are
496 proposed to enrich theoretical research on the translational landslide. The following conclusions
497 are drawn:

498 (1) The characteristics, formation conditions, and occurrence mechanism of rainfall-triggered
499 translational plate-shaped landslides are summarized herein. Such landslides generally exists in a
500 consequent slope with the inclination angle of the sliding surface being less than 10 °, and a group
501 of long and straight structural planes parallel to the slope cuts the slope into several thin plates.
502 The plate-shaped sliding body generally contains extremely thick sandstone, which is nearly
503 horizontal and has good integrity. The bottom sliding zone is a weak mudstone interlayer affected
504 by periodic rainfalls. In addition, single-stage or multistage plate-shaped sliding bodies slide
505 horizontally along the bottom mudstone sliding zone.

(2) Based the mechanical model of the plate-shaped sliding bodies, the relationship between the stability coefficient of the multistage sliding body, K, and the pore-water level, h, was obtained, and the maximum pore-water level, h_{cr}, which causes the instability of multi-stage plate girders was calculated. The instability conditions of the plate-shaped sliding bodies were also determined.

(3) Theoretical conclusions of the plate-shaped landslide research were verified using the long-term monitoring data. The multiparameter monitoring data show that the stability of the sliding body is considerably affected by the rainfall intensity and pore-water pressure. The pore-water pressure in the crack is positive for the beginning of the plate-shaped sliding body, which demonstrates the rainfall-triggered failure mode of the translational landslide. This study compares and analyzes the measured maximum pore-water level $h_{cr}^{'}$ and theoretical calculated value h_{cr}, and discusses the influence in the change of internal cohesive force and internal friction angle on the stability coefficient of the sliding body.

(4) Combined with landslide numerical simulation, this study analyzes and explores the deformation and failure modes of the plate-shaped landslide, i.e., combined with the pore-water pressure in the crack and seepage effect in monsoon, the sliding bodies will slide horizontally along the contact surface of the bottom sand-mud rock weak layer. During the non-rainy season, the pore-water pressure decreases and disappears; the sliding body, owing to its dead weight, will be inclined to the trailing edge. On this basis, this study proposes an optimized monitoring methodology to closely monitor the pore-water pressure, rainfall, and landslide frontal displacement during monsoon, proposed method focuses on the overall inclination angle change of the plate girder during the non-rainy season.

Acknowledgments

We thank Dr. Long Chen at the Institute of Exploration Technology of CAGS for providing landslide monitoring data. This work was supported by the National Natural Science Foundation of China (41804089), Project of Observation Instrument Development for Integrated Geophysical Field of China Mainland (Y201802), and CGS of China Geological Survey Project (1212011220169 and 12120113011100).

References

Barlow, J., Martin, Y., Franklin, S. E.: Detecting translational landslide scars using segmentation of Landsat ETM+ and DEM data in the northern Cascade Mountains, British Columbia, Canadian Journal of Remote Sensing, 29(4):510-517, 2003.

Bellanova, J., Calamita, G., Giocoli, A., Luongo, R., Piscitelli, S.: Electrical resistivity imaging for the characterization of the Montaguto landslide(southern Italy), Engineering Geology, 243(1):272-281, 2018.

Brown, E., Hoek, E.: Trends in relationships between measured in-situ stresses and depth. International Journal of Rock Mechanics and Mining Sciences & Geomechanics Abstracts, 15(4):78-85, 1978.

Chen L., Liu Y., Feng X.: The investigation report on remediation project of Wobaoshi landslide, Sanhui Town, Enyang District, Bazhong City, The Institute of Exploration Technology of

547 CAGS, Chengdu, Open File Rep., pp.57, 2015.

548 Cruden, D.M., Varnes, D.J.: Landslides investigation and mitigation, Special Report 247,
549 Transportation Research Board, National Research Council [R]. [S. l.]:[s. n.], 1996.

550 Darve F., Vardoulakis I.: Degradations and Instabilities in Geomaterials, Springer Vienna, Austria,
551 2004.

552 Emelyanova E.II.: The basic rule of landslide movement, Chongqing Publishing House, Chongqing,
553 China, 1986.

554 Fan, X., Xu, Q., Zhang, Z., et al: The genetic mechanism of a translational landslide, Bulletin of
555 Engineering Geology and the Environment, 68(2):231-244, 2009.

556 Fan, X.: Mechanism and remediation measures for translational landslide [M. S. Thesis], Chengdu:
557 Chengdu University of Technology, 2007.

558 Fan X., Xu Q., Zhang Z., et al: Study of genetic mechanism of translational landslide, Chinese Journal
559 of Rock Mechanics and Engineering, 27(Supp.2):3753-3759, 2008.

560 Griffiths, D. V., Lane, P. A.: Slope stability analysis by finite elements, Géotechnique, 49(3), 387-403,
561 1999.

562 Guzzetti, F., Cardinali, M., Reichenbach P., et al.: Landslides triggered by the 23 November 2000
563 rainfall event in the Imperia Province, Western Liguria, Italy, Engineering Geology,
564 73(3-4):229-245, 2004.

565 Guo X., Huang R., Deng H., Xu Q., ZHAI G.: Formation and mechanism analysis of multi-level rift
566 trough in translational sliding landslide, Journal of Engineering Geology, 21(5):770-778, 2013.

Labuz J. F., Zang A.: Mohr–Coulomb Failure Criterion, Rock Mechanics and Rock Engineering, (2012)45:975–979, 2012.

Lin J. Yang W., Bao C.: Progressive collapse mechanism of hybrid structures with different vertical stiffness, China Earthquake Engineering Journal, 40(4):713-720, 2018.

Liu Y., Wang J.: The research and application of landslide surface crack monitoring method based on laser ranging mode, Environmental and Earth Sciences Research Journal, 2(2):19-24, 2015.

Martin, Y. E., Franklin, S. E.: Classification of soil- and bedrock-dominated landslides in British Columbia using segmentation of satellite imagery and DEM data, International Journal of Remote Sensing, 26(7):1505-1509, 2005.

Matjaž, M., Matja, C., Mitja, B.: Hydrologic conditions responsible for triggering the Stože landslide, Slovenia, Engineering Geology, 73(3-4):193-213, 2004.

Mario, F., Francesca, B.: Evaluation of landslide reactivation: a modified rainfall threshold model based on historical records of rainfall and landslides, Geomorphology, 94(1-2): 40-57, 2008.

Sergio, D. N., Lourenco, K. S., Hiroshi, F.: Failure process and hydrologic response of a two layer physical model: Implications for rainfall-induced landslides, Geomorphology, 73(1-2):115-130, 2006.

Teixeira, M., Bateira, C., Marques, F., et al: Physically based shallow translational landslide susceptibility analysis in Tibo catchment, NW of Portugal, Landslides, 12(3):455-468, 2015.

Tschuchnigg, F., Schweiger, H.F. & Sloan, et al: Slope stability analysis by means of finite element limit analysis and finite element strength reduction techniques. Part I: Numerical studies

considering non-associated plasticity, Computers and Geotechnics, 70, 169-177, 2015.

Tschuchnigg, F., Schweiger, H.F., Sloan, S.W., et al: Comparison of finite-element limit analysis and strength reduction techniques, Géotechnique, 65(4), 249-257, 2015.

Wang L.，Zhang Z.: The mechanical patterns of the deformation in rock slope, Geological Publishing House, Beijing, China, 1985.

Xu Q., Zeng Y.: Research on acceleration variation characteristics of creep landslide and early-warning prediction indicator of critical sliding, Chinese Journal of Rock Mechanics and Engineering, 28(6):1099-1106, 2009.

Xu Q., Huang R., Liu T., et al.: Study of the formation mechanism and design of control engineering for the super-huge Tiantai landslide, IAEG2006 Engineering Geology for Tomorrow Cities, Sichuan province, China, 2006, 602.

Xu Q., Fan X., Li Y., Zhang S.: Formation condition, genetic mechanism and treatment measures of plate-shaped landslide, Chinese Journal of Rock Mechanics and Engineering, 29(2):242-250, 2010.

Yin K., Jian W., Zhou C., et al: Study on the mechanism of the translational landslide in Wanzhou district and prevention project, Wuhan: China University of Geosciences，Open File, pp.153-154, 2005.

Zhang L., Pei X., Lin H., Li S.: Evolution of Landslide Based on Growth Characteristics of Trees on the Landslide, Mountain Research, 33(4):503-510, 2015.

Zhang Z., Wang S., Wang L.: The analytical principle on engineering geology, Geological Publishing

607 House, Beijing, China, 1994.

608 **Figure Captions**

609 Fig. 1. Geographical location and elevation map of the Wobaoshi landslide.

610 Fig. 2. Topographic map of the Wobaoshi landslide and photographs of observation
611 points: (a) exposed bedrock at the front edge; (b) the houses had cracked at the front
612 edge (c) the roadbed is pushed uplifted at the front edge; (d) crack II and bent trees;
613 and (e) crack I.

614 Fig. 3. I- I′ sectional graph of the landslide.

615 Fig. 4. Layout planar graph of the monitoring equipment.

616 Fig. 5. Photos of installation the monitoring instruments: (a) crack I gauge; (b) rain
617 gauge and pore-water pressure gauge; and (c) crack II gauge.

618 Fig. 6. Monitoring data curves (rainfall intensity and width of cracks I and II).

619 Fig. 7. Monitoring data curves: (a) width of crack I and its pore-water pressure; (b)
620 width of crack II and its pore-water pressure.

621 Fig. 8. Absolute slippage amount curves of cracks I and II.

622 Fig. 9. Geomechanical model of two-stage plate-shaped sliding bodies.

623 Fig. 10 Determination of the maximum measured pore-water level $h_{cr}^{'}$.

624 Fig. 11. Comparison figure of $h_{cr}^{'}$ (measured) and h_{cr} (theoretical).

625 Fig. 12 Example of finite element simulation and numerical calculation.

626 Fig. 13 Schematic of the deformation and failure mode of the Wobaoshi landslide.

627

Table

Table 1 Typical monitoring data of the Wobaoshi landslide

Measurement duration	Crack I width (m)	Crack II width (m)	Crack I Pore-water pressure (kPa)	Crack II Pore-water pressure (kPa)
2015/2/1	5.640	4.492	0	0
2015/4/24	5.945	4.774	18.561	27.303
2015/5/7	5.886	4.798	18.649	33.212
2015/5/13	6.203	4.810	33.134	33.036
2015/5/15	6.215	4.899	34.476	35.456
2015/8/15	6.350	5.451	41.474	31.625
2015/9/14	6.330	5.380	34.594	30.772
2015/11/15	5.871	4.952	11.280	17.395
2016/2/15	5.790	4.599	0	0
2016/4/13	5.824	4.706	10.378	26.156
2016/5/14	6.173	4.850	33.810	36.035
2016/7/17	6.161	5.281	36.162	31.664
2016/8/18	6.310	5.220	38.024	33.683
2016/9/15	6.325	5.251	39.298	29.723
2016/12/20	5.960	4.763	5.106	0
2017/2/16	5.865	4.770	0	0
2017/4/13	5.984	5.152	24.108	29.155
2017/5/17	6.118	5.332	43.463	31.703
2017/7/17	6.433	5.239	42.787	30.478
2017/8/15	6.490	5.255	43.639	29.273
2017/11/14	6.091	5.004	5.488	8.428
2017/12/20	5.922	4.723	0	0
2018/1/11	5.881	4.751	0	0
2018/4/10	6.194	5.110	33.957	35.819
2018/5/17	6.283	5.246	33.830	33.438
2018/6/16	6.452	5.315	36.995	28.391
2018/7/10	6.421	5.310	38.171	29.841

Table 2 Rainfall intensity value of the Wobaoshi landslide (mm/month)

Year \ Month	1	2	3	4	5	6	7	8	9	10	11	12	Total
2015		13.5	30.5	71.8	121.9	165.0	240.1	163.0	166.1	85.0	39.6	14.1	1110.6
2016	6.9	12.5	26.5	56.8	98.4	126.1	193.2	155.1	150.0	90.3	29.1	13.5	958.4
2017	5.7	16.8	36.8	90.5	115.6	185.1	271.3	190.0	176.2	109	52.1	20.8	1269.9
2018	11.5	10.9	31.5	99.9	121.0	205.1	191.6	\	\	\	\	\	671.5

633 Table 3 Measured pore-water level data of the sliding bodies

Measured time	Crack Ⅰ slippage (m)	Measured pore-water level (m)	Crack II slippage (m)	Measured pore-water level (m)
2015/4/15	0.072	14.566	0.183	12.736
2015/4/24	0.305	15.174	0.282	12.936
2015/5/7	0.246	15.183	0.306	13.539
2015/5/13	0.561	16.661	0.318	13.521
2015/5/15	0.573	16.798	0.407	13.768
2015/6/20	0.711	17.032	0.888	13.502
2015/7/17	0.519	17.474	0.798	13.471
2015/10/16	0.481	16.470	0.538	13.340
2015/11/15	0.229	14.431	0.458	11.925
2016/1/15	0.108	\	0.169	\
2016/4/13	0.184	13.490	0.214	12.819
2016/4/23	0.421	14.339	0.269	12.804
2016/4/29	0.475	16.214	0.432	13.835
2016/5/11	0.469	16.494	0.449	13.920
2016/5/14	0.531	16.505	0.358	13.827
2016/6/15	0.508	16.731	0.618	13.574
2016/9/15	0.683	17.312	0.758	13.183
2016/10/12	0.637	14.930	0.618	12.360
2017/2/16	0.223	\	0.278	\
2017/4/13	0.344	15.741	0.658	13.125
2017/4/29	0.489	16.712	0.686	13.141
2017/5/2	0.518	16.799	0.648	13.024
2017/5/13	0.501	16.877	0.734	13.161
2017/5/17	0.476	17.715	0.838	13.385
2017/8/15	0.848	17.733	0.758	13.137
2017/9/16	0.869	16.324	0.333	12.235
2018/3/14	0.281	\	0.618	11.013
2018/4/10	0.552	16.745	0.754	13.805
2018/5/17	0.643	16.732	0.333	13.562

634

635 Table 4 Mechanical parameters of the sliding body model

Lithology	Elastic Modulus (N/m^2)	Poisson Ratio	Gravity (N)	Internal Cohesion (N/m^2)	Internal Friction Angle	Permeability Coefficient (cm/s)
Arkose	600000	0.25	19200	30000	36°	1.20E-07
Silty Mudstone	360000	0.28	19000	20000	30°	6.00E-07
Clay	300000	0.3	18000	10200	11.2°	1.20E-06

636

637

638 Table 5 Loading steps of the water level in Crack I and II in FEM model

Loading Steps	Crack I	Crack II
0	314.50 m	311.00 m
1	316.00 m	313.00 m
2	317.50 m	315.00 m
3	316.00 m	313.00 m
4	314.50 m	311.00 m

639